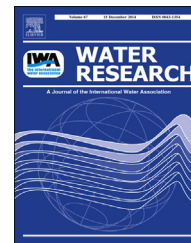


Available online at www.sciencedirect.com

ScienceDirect

journal homepage: www.elsevier.com/locate/watres

Adsorptive removal of methylene blue by rhamnolipid-functionalized graphene oxide from wastewater

Zhibin Wu ^{a,b}, Hua Zhong ^{a,b,c,**}, Xingzhong Yuan ^{a,b,*}, Hou Wang ^{a,b},
Lele Wang ^{a,b}, Xiaohong Chen ^d, Guangming Zeng ^{a,b}, Yan Wu ^e

^a College of Environmental Science and Engineering, Hunan University, Changsha 410082, PR China

^b Key Laboratory of Environment Biology and Pollution Control, Hunan University, Ministry of Education, Changsha 410082, PR China

^c Department of Soil, Water and Environmental Science, The University of Arizona, Tucson AZ85719, USA

^d School of Business, Central South University, Changsha 410083, PR China

^e College of Environment and Energy, South China University of Technology Guangzhou 510006, PR China

ARTICLE INFO

Article history:

Received 19 April 2014

Received in revised form

4 September 2014

Accepted 19 September 2014

Available online 2 October 2014

Keywords:

Adsorption

Rhamnolipid-functionalized graphene oxide

Methylene blue

Adsorption kinetics

Adsorption isotherms

ABSTRACT

In this article, a rhamnolipid-functionalized graphene oxide (RL-GO) hybrid was prepared by one-step ultrasonication and adsorptive removal of methylene blue (MB) from both artificial and real wastewater by the RL-GO was investigated. The Scanning electron microscopy (SEM), Transmission electron microscopy (TEM), Fourier transform infrared spectrum (FT-IR), X-ray diffraction (XRD), X-ray photoelectron spectroscopy (XPS), Brunauer–Emmett–Teller (BET) area and Zeta potential analysis were used to characterize the adsorbent. The results showed that RL-GO had abundant functional groups and a mesopores feature. MB adsorption by the RL-GO increased with increase in adsorbent dose, pH, temperature and initial MB concentration, while it was insensitive to ionic strength variation. The adsorption kinetics fitted well to the pseudo-second-order model with correlation coefficients greater than 0.999. The Intra-particle diffusion and Boyd's film-diffusion models showed that the rate-controlled step was dominated by film-diffusion in the beginning and then followed by intra-particle diffusion. The adsorption isotherm was fitted by adsorption models with the suitability in order of BET > Freundlich > Langmuir > Temkin, based on comparison between correlation coefficients. Thermodynamic analysis of equilibriums suggested that the adsorption MB on RL-GO was spontaneous and endothermic. The adsorption mechanism was also proposed to be electrostatic attraction, π – π interaction and hydrogen bond. In addition, the real wastewater experiment, the regeneration study and the comparative cost analysis showed that the RL-GO composites could be a cost-effective and promising sorbent for MB wastewater treatment owing to its high efficiency and excellent reusability.

© 2014 Elsevier Ltd. All rights reserved.

* Corresponding author. College of Environmental Science and Engineering, Hunan University, Changsha 410082, PR China. Tel.: +86 731 88664182; fax: +86 731 88823701.

** Corresponding author. College of Environmental Science and Engineering, Hunan University, Changsha 410082, PR China. Tel./fax: +86 731 88821413.

E-mail addresses: zhonghua@hnu.edu.cn (H. Zhong), yxz@hnu.edu.cn (X. Yuan).

<http://dx.doi.org/10.1016/j.watres.2014.09.026>

0043-1354/© 2014 Elsevier Ltd. All rights reserved.

1. Introduction

Dyes and pigments are widely used in the leather and textile dyeing, food technology, pharmaceutical, and cosmetic industries (Gusmao et al., 2013; Liu et al., 2011). It is reported that over 100,000 different commercial dyes and pigments exist, and each year over 7×10^5 tons of dyestuffs are produced. Release of the dyes to the environment have aroused serious concerns all over the world for the toxic effects of dyeing effluents, such as mutagenic and carcinogenic action to aquatic biota and humans (Anbia and Salehi, 2012; Nethaji et al., 2010). Therefore, removing the dyes from wastewater to an acceptable level before discharging into the natural environment is a challenge for industries.

At present, several physicochemical and biological methods, including catalytic degradation (Ghosh et al., 2013), photo-catalytic degradation (Dong et al., 2010), biodegradation (Ong et al., 2005), membrane filtration (Wu et al., 1998) and adsorption (Luo et al., 2010) have been developed to lessen dye's pollution and hazards. Among these methods, adsorption is considered as an attractive and favorable technique because its low costs, easy operation and high efficiency. Heretofore, numerous carbon-based materials have been used for dyes adsorption applications, such as rice husk (Chowdhury et al., 2011), sawdust (Khattri and Singh, 2009), activated carbon (Yener et al., 2008) and carbon nanotubes (Yao et al., 2010). Last several years, much attention focused on emerging material graphene.

Graphene, a novel one-atom-thick two-dimensional graphitic carbon system with sp^2 -bonded carbon localized on a honeycomb lattice (Chang et al., 2012; Tang et al., 2013; Yan et al., 2012), has been under intense multidisciplinary study attributed to its extraordinary electrical and mechanical properties, large surface area, excellent mobility of charge carriers, and good thermal conductivity (Wang et al., 2013a; Xu et al., 2012; Zhao et al., 2012). Following this trend, graphene oxide (GO) has attracted more and more attention owing to its role as a precursor for the cost-effective mass production of graphene-based materials.

GO is referred to a strongly oxygenated, highly hydrophilic layered material that can be readily exfoliated in water to yield stable dispersions consisting mostly of single layer sheet (Paredes et al., 2008). Recent researches have proved that GO could be a promising material to adsorb pollutants from water, due to its large surface area and surface oxygen-containing groups (Wang et al., 2013b; Zhao et al., 2011a). For examples, graphene oxide was used as an adsorbent for heavy metal removal in our previous study and it was found that the adsorption capacity of GO for Zn(II) could reach up to 246 mg/g (Wang et al., 2013b). G.K. Ramesha et al. demonstrated that exfoliated graphene oxide (EGO) can act as good adsorbents and it showed removal efficiency of up to 95% for cationic dyes (Ramesha et al., 2011). The adsorption of methylene blue (MB) onto GO from aqueous solution was investigated in many studies (Li et al., 2013a; Yang et al., 2011; Zhang et al., 2011). Although quite a few functionalized GO have been developed, the adsorption capacity for MB of these functionalized GO is still low (Fan et al., 2012; Li et al., 2013b). Some limitations for use of GO are the high water absorption and the poor

performance of the solid–liquid separation. It will cause a risk of exposure to humans, animals and aquatic organisms if GO remains in the filtered water (Bianco, 2013; Chen et al., 2012; Wang et al., 2011). Thus, it remains as a challenge to develop the high adsorption capacity, good chemical stability and easy solid–liquid separation graphene-based materials for MB wastewater treatment.

Recently, chemical surfactants have been employed in improving the adsorption ability, enhancing the biocompatibility and reinforcing the photo-catalytic performance of graphene based materials owing to the capability of surfactants to prevent aggregation (Lin et al., 2011; Qu et al., 2013; Zhao et al., 2014; Zhu et al., 2013). In our previous studies, cetyltrimethylammonium bromide (CTAB) was selected to modify graphene (GN), and the results showed that the CTAB groups together with $-OH$ and $-COOH$ groups on the GN surface can make CTAB-GN be a good adsorbent for removal of Cr(VI) in aqueous solutions (Wu et al., 2013). Rhamnolipid (RL), a glycolipid-type biosurfactant, is produced primarily by *Pseudomonas aeruginosa* with high interfacial activity and environmental compatibility (Asci et al., 2008). To our best knowledge, the report about assistance of rhamnolipid in improving dyes adsorption by graphene oxide remains scarce. In this study, the rhamnolipid modified graphene oxide (RL-GO) was prepared and characterized. The adsorption behavior of methylene blue (MB) to RL-GO, including the adsorption kinetics, isotherms, thermodynamics, mechanisms and the factors potentially affecting the adsorption were investigated. Finally, the application of RL-GO hybrid to real MB wastewater and the cost analysis on the fabrication of RL-GO were also performed.

2. Materials and methods

2.1. Materials

Rhamnolipid (>90%) was purchased from Zijin biological technology Co, Ltd (Huzhou, China). MB (methylene blue trihydrate, $C_{16}H_{18}ClN_3S \cdot 3H_2O$, 99% in purity) was produced by Tianjin Hengxing Chemical Reagent Co, Ltd (Tianjin, China) and its molecular structure and pKa value were shown in Fig. 1. The 1-ethyl-3-(3-dimethylaminopropyl) carbodiimide hydrochloride (EDC), 4-(dimethylamino) pyridine (DMAP) and N,N-Dimethylformamide (DMF) were supplied by Aladdin Industrial Corporation (Shanghai, China). River water was taken from Xiangjiang River located in Changsha, Hunan province, China. Dye wastewater with COD between 400 and 600 mg/L was obtained from a textile mill in Dongguan, Guangdong province, China. All other chemicals were analytical grade

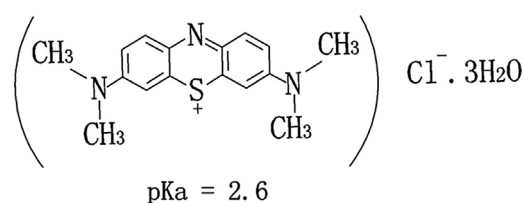
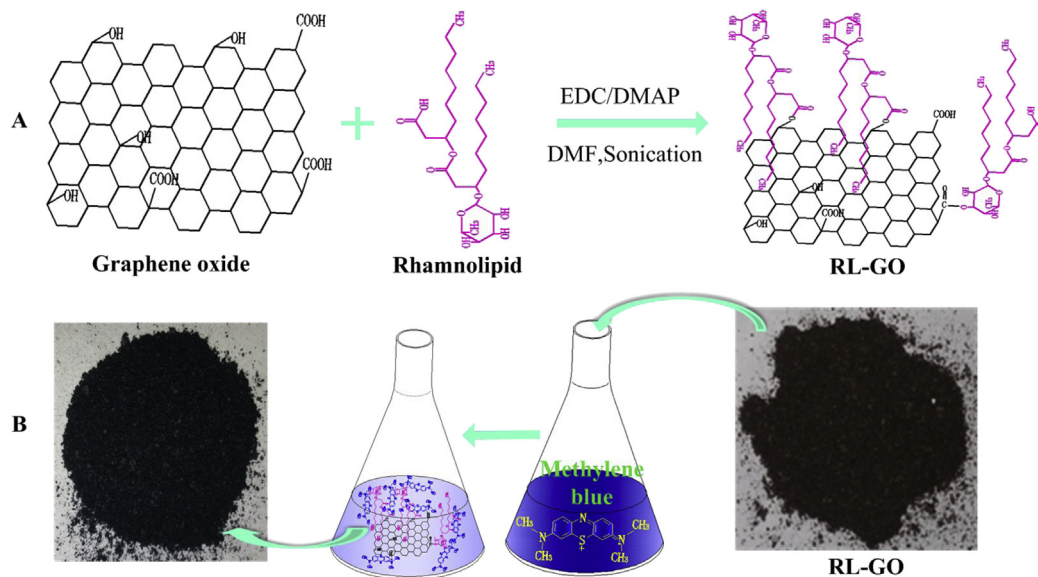


Fig. 1 – Molecular structures of methylene blue (MB).



Scheme 1 – Schematic depiction of the formation of RL-GO and application for removal of MB.

and used as received. All solutions were diluted preparation using ultra-pure water.

2.2. Preparation of graphene oxide

Graphene oxide was prepared from graphite powder (particle size ≤ 30 μm , Tianjin Kermel Chemical Regent Ltd, China) by a modified Hummers method (Hummers and Offeman, 1958). Briefly, graphite (2.0 g) and NaNO_3 (1 g) were placed in a 250 mL beaker. Then, 46 mL of sulfuric acid (98%) was added with stirring in ice bath. While maintaining the temperature below 283 K, 6 g KMnO_4 and 1 g NaNO_3 were slowly added to the suspension with vigorous stirring. After stirred for 2 h in ice-bath, the mixture was stirred at 303 K for 30 min. As the reaction proceeded, the color of the mixture gradually changed to brownish paste. Next, the paste was diluted with 92 mL ultra-pure water under vigorous agitation, heated to 368 K and then maintained for 30 min. By then the color of the suspension changed to bright yellow. When the suspension was allowed to cooled to 333 K, 10 mL H_2O_2 (30 wt.%) solution was added to the mixture to terminate the reaction and the mixture was stirred for 2 h at room temperature. After centrifugation, the precipitate was washed repeatedly with 5% HCl to remove residual metal ions, and then with de-ionized water to remove the sulfate ion. Finally, the precipitate (graphite oxide) was bath sonicated and dried under vacuum at 338 K.

2.3. Synthesis of RL-GO composites

The RL-GO hybrid was prepared by one-step ultrasonication as shown in Scheme 1A. In brief, 200 mg GO was dissolved into 100 mL DMF and bath sonicated for 1 h. Then 600 mg rhamnolipid was added into the GO suspension and sonicated with stirring until rhamnolipid completely dissolved. Next, N-(3-dimethylaminopropyl)-N-ethylcarbodiimide hydrochloride

(1 g) and 4-(dimethylamino) pyridine (200 mg) were added. The reaction was allowed to progress under stirring and ultrasonication for over 3 h. After that, the suspension was precipitated with methanol under vigorous stirring. The black solid precipitate (RL-GO) was centrifuged and washed with anhydrous ethanol five times, and then with ultrapure water twice. Finally, rhamnolipid-functionalized graphene oxide composite was freeze-dried under vacuum and used for adsorption.

2.4. Characterization methods

The surface morphologies of adsorption materials were observed by the field emission scanning electron microscope (SEM, JSM-6700F, Japan) and transmission electron microscopy (TEM, JEM-3010, Japan). Fourier transform infrared spectrum (FT-IR) measurements were carried out by using Nicolet 5700 Spectrometer in KBr pellet at room temperature. The X-ray diffraction (XRD) patterns were recorded with Bruker AXS D8 Advance diffractometer using Cu-K α source ($\lambda = 1.541$ \AA). The Brunauer–Emmett–Teller (BET) specific surface area and pore size were measured by using automatic surface analyzer (Quantachrome, USA). The surface elemental composition analyses were conducted based on the XPS spectra (Thermo Fisher Scientific-K-Alpha 1063, UK) with a resolution of 0.5 eV. The zeta potentials analysis of adsorbent in water solutions at pH 3.0–11.0 (adjust by NaOH or HCl) was determined with a zeta potential meter (Zetasizer Nano-ZS90, Malvern).

2.5. The adsorption of methylene blue (MB)

The schematic diagram of RL-GO for MB adsorption was shown in Scheme 1B. All batch experiments of MB adsorption were carried out in 50 mL Erlenmeyer flask with a temperature controlled water bath shaker at an agitation speed of 170 rpm.

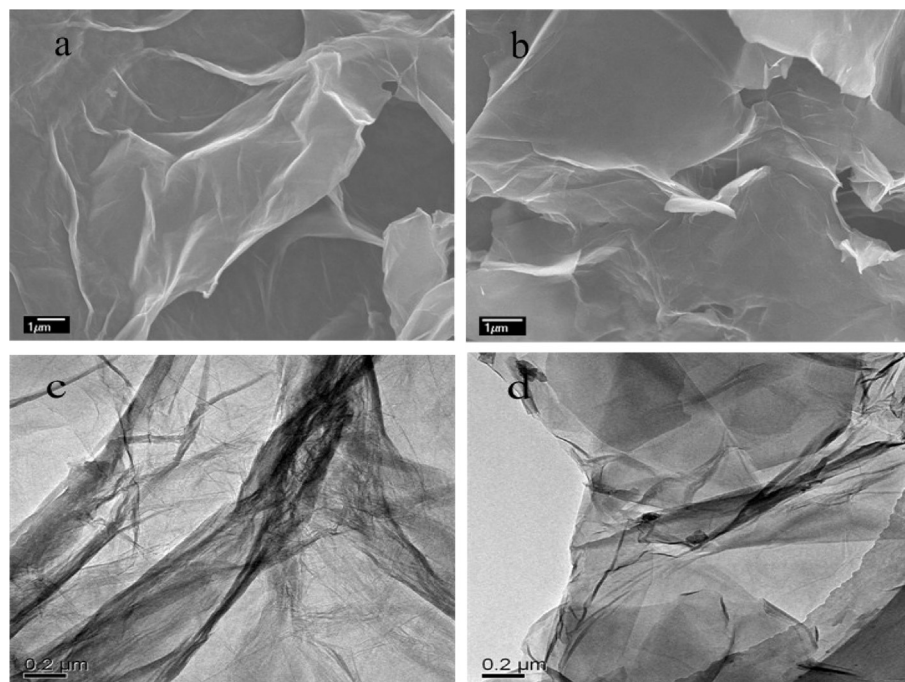


Fig. 2 – The SEM images of GO (a) and RL-GO (b); The TEM images of GO (c) and RL-GO (d).

The desired pH value of solutions was adjusted with 0.1 M NaOH or 0.1 M HCl using a pH meter (PHSJ-5, China).

To investigate the effect of adsorbent dosage on the adsorption of MB, various adsorbent dosages from 5 mg to 25 mg were added to 25 mL of solution with MB initial concentration of 200 mg/L, and then the flasks were shaken under 298 K for 24 h. The effect of pH on adsorption of MB was studied in a pH range of 3.0–11.0 by agitating 25 mL of 200 mg/L MB solutions with RL-GO of 400 mg/L at 298 K for 24 h. For kinetics studies, 200 mg of RL-GO was added to 500 mL methylene blue solutions of concentrations 100–200 mg/L in flask at pH 7.0. The agitation speed and the temperature were controlled at 170 rpm and 298 K, respectively. The samples were taken from the flasks using pipette at predetermined time intervals (from 5 min to 24 h).

The adsorption isotherms experiments were performed at different temperatures. 25 mL of MB solution with concentration varying from 50 to 400 mg/L was adjusted on pH to 7.0 and then added with 10 mg RL-GO adsorbent for shaking 24 h. In order to investigate the effect of ionic strength on the adsorption of MB, 10 mg of RL-GO was added to 25 mL of MB (100 mg/L or 200 mg/L) solution containing 0–0.12 mol/L NaCl. The pH of the MB solution was adjusted to 7.0 and the suspension was shaken at 298 K for 24 h. The study on application of RL-GO to real water samples was carried out by adding 10 mg of RL-GO to 25 mL of MB (100 mg/L or 200 mg/L) in real wastewater and shaking the mixture at 298 K for 24 h. The regeneration of RL-GO was conducted by adding MB-loaded RL-GO solids to the mixture of methanol and acetic acid (a mass ratio of 10:1) to a final concentration of 400 mg/L and the mixture was stirred at 298 K and 170 rpm for 30 min. After desorption, the suspension liquid was to undergo

centrifugation. The same step was repeated for three times and the final precipitant was dried at 353 K for reuse. In each cycle of adsorption test, suspension containing 400 mg/L of RL-GO and 200 mg/L of MB was shaken at 298 K for 24 h with no pH adjustment.

2.6. Measurement of MB concentration

All adsorption experiments were performed in triplicates and the results were reproducible within 5%. After reaction, the samples were subjected to solid–liquid separation. The liquid samples after separation were analyzed to determine the residual MB concentration by UV spectrophotometer (UV-2550, SHIMADZU, Japan) at 665 nm. The amount of MB adsorbed onto RL-GO at equilibrium was calculated using the following equation:

$$q_e = \frac{C_0 - C_e}{m} V \quad (1)$$

where q_e is the adsorption quantity (mg/g); C_0 and C_e is the initial and equilibrium concentrations of MB in solution (mg/L), respectively; V is the volume of solution (L), and m is the weight of RL-GO (g).

3. Result and discussion

3.1. Characterization of RL-GO composite

Fig. 2 shows the SEM and TEM images of GO and RL-GO. It is apparently that there are many crumplings on the surface of GO which come from the scrolling of GO sheets (Fig. 2a). This is

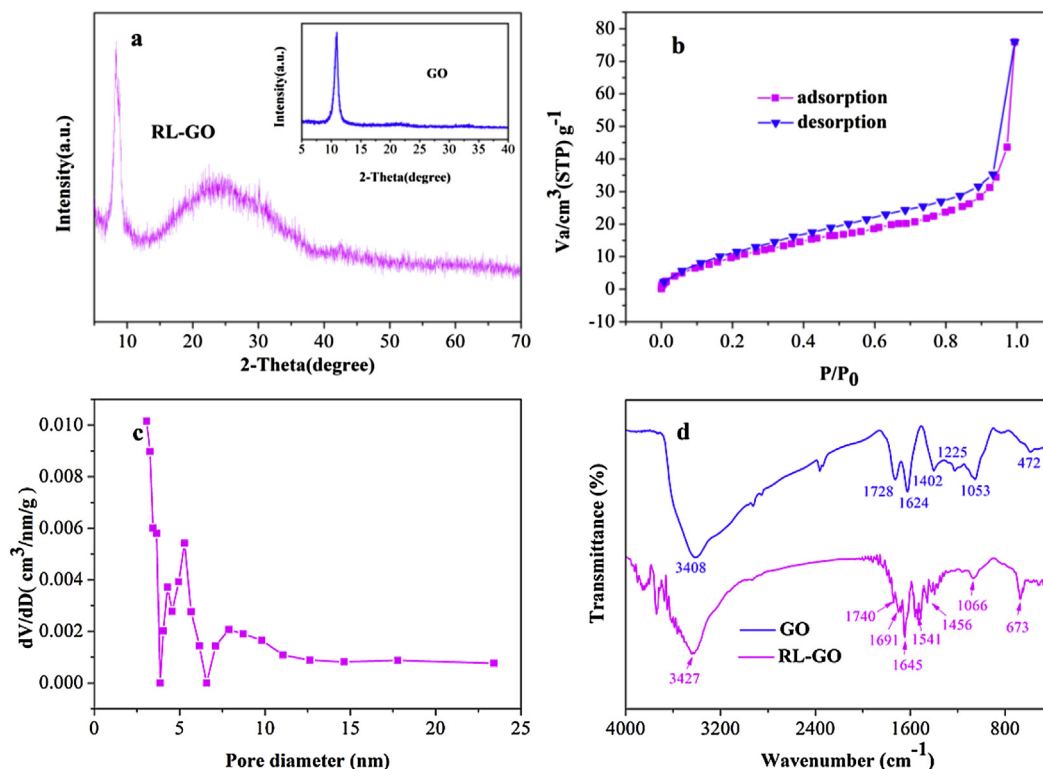


Fig. 3 – (a) The XRD patterns of GO and RL-GO; (b) N_2 adsorption–desorption isotherms of RL-GO at 77 K and (c) pore-size-distribution curve of RL-GO; (d) The FT-IR spectrums of GO and RL-GO.

similar to what was observed by Li et al. (Li et al., 2013a). In contrast, the RL-GO (Fig. 2b) has a relative smooth surface. This indicates that the existence of biosurfactant rhamnolipid can effectively inhibit the agglomeration of graphene oxide which may make GO layer easier to peel off by ultrasonication. The further proof is supported by TEM images of GO and GO-RL in Fig. 2c and d, respectively. It can be observed that there are much more small crimple regions on GO than on sheet-like RL-GO.

The internal structures of both GO and RL-GO nanoplatelets were also examined by XRD and the results are shown in Fig. 3a. A typical sharp diffraction peak of GO is observed at $2\theta = 10.9^\circ$, corresponding to the interlayer spacing of 0.81 nm (Wang et al., 2013b). For the XRD patterns of RL-GO, the relatively broad diffraction peak centers at $2\theta = 8.45^\circ$ with 1.05 nm d-spacing. The layer distance increases from 0.81 nm to 1.05 nm after GO composited with rhamnolipid, which may be ascribed to the introduction of more oxygen-containing functional group on the surface of RL-GO. Besides, a new wide peak at $2\theta = 24.5^\circ$, which corresponds to the normal graphene diffraction peak with 0.363 nm d-spacing, is observed in the XRD pattern of RL-GO (Liu et al., 2013). This may be due to the partial reduction of GO after modified.

As shown in Fig. 3b, the N_2 adsorption–desorption isotherm of RL-GO can be categorized as type IV with a hysteresis loop at relative pressure (P/P_0) between 0.4 and 1.0, indicating a mesoporous structure of RL-GO (Ai and Jiang, 2012). The corresponding porosity distribution of RL-GO is shown in Fig. 3c. The average pore diameter is calculated to be 3.069 nm by the Barret–Joyner–Halenda (BJH) model, with

which the pore size distributions concentrates in the mesopores (2–50 nm in size). A specific surface area of $42.46 \text{ m}^2/\text{g}$ for RL-GO is obtained using Brunauer–Emmett–Teller (BET) equation.

In order to verify above viewpoints, the element characterization of sample was analyzed by FT-IR and XPS. The FT-IR spectrums of GO and RL-GO are shown in Fig. 3d. Several characteristic FT-IR peaks of GO are observed, for examples, O–H (3408 cm^{-1}), C=O (1728 and 1402 cm^{-1}), C=C (1624 cm^{-1}), C–OH (1225 cm^{-1}), C–O–C (1053 cm^{-1}) and C–O (472 cm^{-1}). Similarly, in the FT-IR spectrum of RL-GO, the same functional groups above mentioned are found around the corresponding wavenumber. However, the peak of C–OH (1225 cm^{-1}) disappeared for RL-GO, the C–H vibration of rhamnolipid hydrocarbon (1456 cm^{-1}) and the peak of C=O (1541 and 1691 cm^{-1}) for ester or –COOH emerged, indicating successful binding of rhamnolipid to GO.

The full scan XPS spectrums shows the presence of C and O element at the binding energy of 284.67 eV and 532.88 eV for GO (Fig. 4a), and 284.66 eV and 532.60 eV for RL-GO (Fig. 4c), respectively. The ratio of carbon content to oxygen content (C/O) for GO is 5.88 and for RL-GO is 5.15, which implies that more oxygen-containing functional groups, such as C–OH, C=O are introduced. This result is consistent with the XRD and FT-IR analysis. Additionally, a computational multi peak resolution method for XPS has been applied to the C1s band of GO and RL-GO. As shown in Fig. 4b, the C1s band of GO can be deconvoluted into four peaks centered at 284.67, 286.39, 288.11, and 289.01 eV, corresponding to the C=C/C–C, C–O, carbonyl and carboxyl groups, respectively (Tiwari et al.,

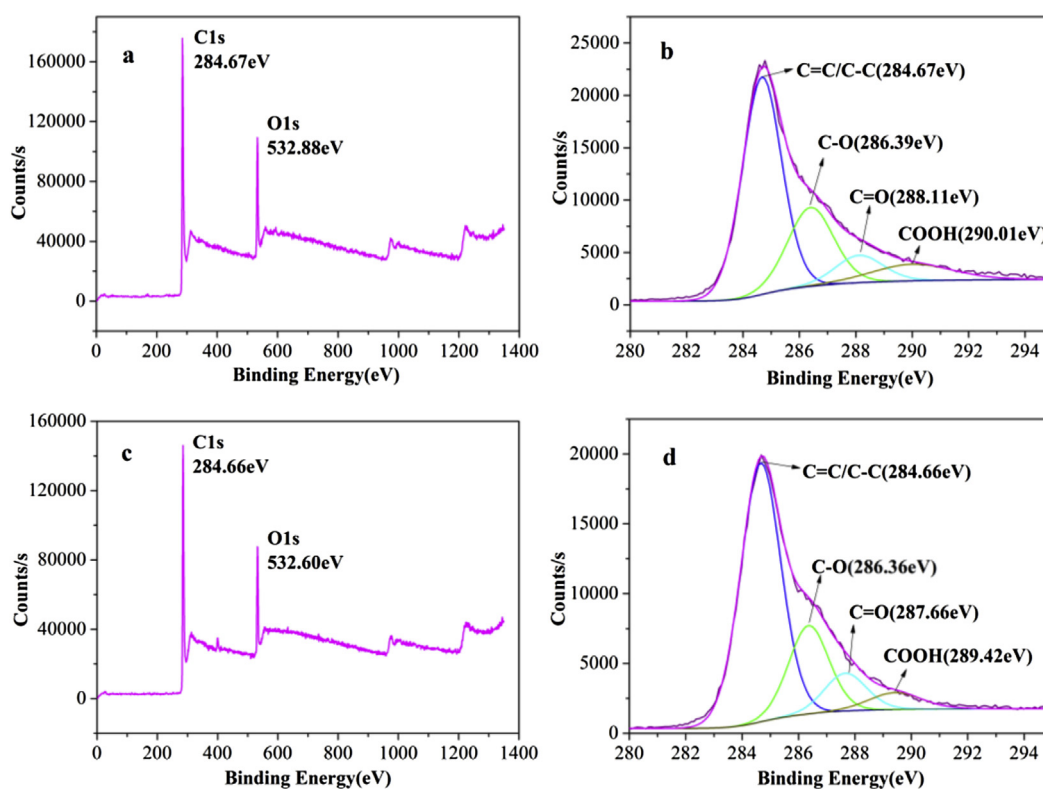


Fig. 4 – (a) XPS survey spectra and (b) C1s core level spectra of GO, (c) XPS survey spectra and (d) C1s core level spectra of RL-GO.

2013). The C1s band of RL-GO (Fig. 4d) also can be deconvoluted into four peaks, corresponding to C=C/C-C (284.66 eV), C-O (286.36 eV), C=O (287.66 eV) and COOH (289.42 eV). These results are agreed with characterization by FT-IR.

3.2. The effect of adsorbent dosage on adsorption of MB

Fig. 5 shows the effects of the RL-GO (or GO) dosage on the adsorption of MB. The removal percentage of MB increases with the RL-GO (or GO) dosage increasing. But further increase the adsorbent dose, the removal percentage increases slightly. It also can be seen that, with the increasing adsorbent dose, the adsorption capacity of MB decreases. This is mainly because a higher adsorbent dosage provides a large excess of the active sites leading to a lower utility of the sites at a certain concentration of MB solution (Li et al., 2013b). In addition, it is apparently that RL-GO is superior to GO in MB adsorption capacity under the experiment conditions. This can be explained by the results, characterized by XRD and XPS, that RL-GO has a larger layer spacing and more oxygen containing functional groups than GO for MB adsorption.

3.3. The effect of pH on MB adsorption

The pH influences dye adsorption by changing the surface charge of the adsorbent and also the speciation distribution of dye in solution phase (Zhang et al., 2011). As shown in Fig. 6, the MB adsorption to RL-GO is sensitive to the pH of the solution. The amount of MB adsorbed onto RL-GO at equilibrium

(q_e) increases from 287.98 mg/g to 499.64 mg/g with the pH increasing from 3 to 11. In particular, the adsorption capacity of the RL-GO for MB increased rapidly in the pH range of 6–8. These results agree with the zeta potential of RL-GO shown in Fig. 6. The pH of point of zero charge (pH_{ZPC}) of RL-GO estimated by zeta potential is about 3.4, and the zeta potential of RL-GO is negative and decreases with increasing pH from 4 to 11 due to dissociation of carboxylic group (-COOH) on RL-GO surface. Electrostatic attraction of between the MB cations and the negatively charged sites on surface of RL-GO is considered to be the major driving force for the adsorption. As

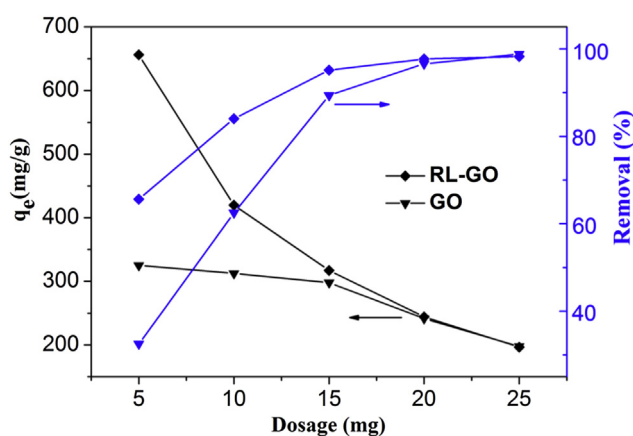


Fig. 5 – Effect of adsorbent dosage on adsorption capacity of MB.

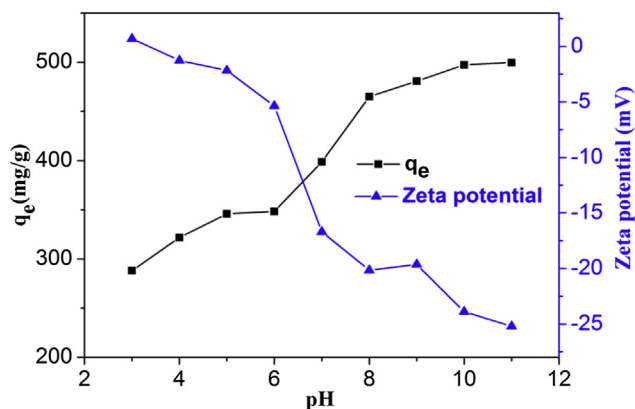


Fig. 6 – Zeta potentials of RL-GO at different pH and effect of pH on adsorption of MB by RL-GO.

a result, increasing pH of the solution enhanced the adsorption.

3.4. The effect of ionic strength on the adsorption capacity

As a high concentration of salts may be included in industrial MB wastewater, and such salts may affect the MB adsorption. Therefore, the influence of salt ionic strength on the removal of MB by RL-GO was studied with the sodium chloride concentration varying from 0 to 0.12 mol/L. The results are shown in Fig. 7. It is found that the adsorption capacity for MB remains almost at the same level with increasing concentration of NaCl. This can be explained by two evenly matched effects of NaCl. On one hand, the salt may cause the adsorption capacity for MB to decrease with increasing NaCl concentration by screening the electrostatic interaction between the MB cations and RL-GO groups. But, on the other hand, the salt has a positive effect for the dissociation of MB molecules to MB^+ by promoting the protonation, and thus resulting in enhancement of the electrostatic interaction between the MB cations and RL-GO groups (Wang et al., 2010).

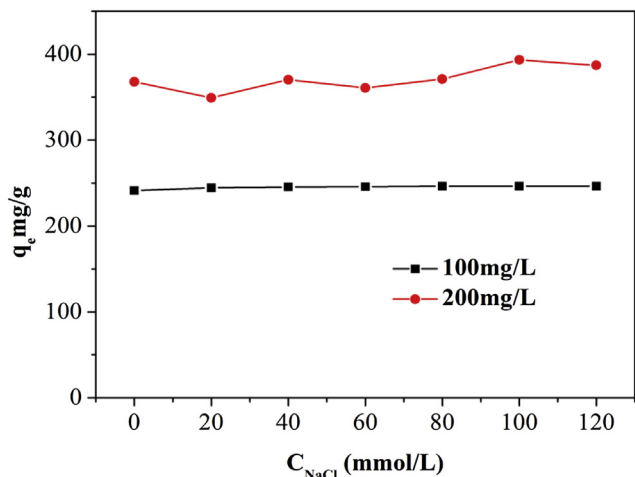


Fig. 7 – The effect of ionic strength on the MB adsorption capacity of RL-GO.

3.5. The effect of temperature and initial MB concentration on adsorption

Fig. 8 shows the relationships between the equilibrium adsorption capacity (q_e) and equilibrium MB concentration (C_e) in solution at different temperatures (298 K, 308 K and 318 K). It can be observed that the temperature remarkably influences the adsorption of MB. The adsorption capacity increases with increasing temperature, which indicates that the adsorption is an endothermic process and high temperature favors the adsorption. Increasing temperature may cause a swelling effect on the porosity and the pore volume of the adsorbent, which enables MB molecules to rapidly diffuse across the external boundary layer and within the internal pores of the RL-GO particle (Chowdhury et al., 2011; Rahchamani et al., 2011). It is also clear that the adsorption capacity increases from 124.96 to 581.56 mg/g with initial MB concentration increases in the range of 50–400 mg/L. The higher initial MB concentration will provide more powerful driving force to overcome the mass transfer resistances between the aqueous and solid phases.

3.6. Adsorption kinetics

To analyze the kinetics of MB adsorption onto RL-GO, the pseudo-first-order, pseudo-second-order, intra-particle diffusion and Boyd's film-diffusion models were examined at three different initial MB concentrations in this study. The pseudo-first-order model was widely used for adsorption process, and its linearized-integral form is as follows (Lagergren, 1898):

$$\log(q_e - q_t) = \log q_e - k_1/2.303t \quad (2)$$

where q_e and q_t is the adsorption capacity of RL-GO for MB at equilibrium and any instant of time t (h), respectively. k_1 is the rate constant of pseudo-first-order adsorption (h^{-1}). k_1 and q_e is calculated from the slope and intercept of the plots of $\log(q_e - q_t)$ versus t , respectively. The related parameters are presented in Table 1. There is a significant difference between the calculated q_e and the experimental q_e . The low correlation coefficient R^2 also shows that the adsorption of MB onto RL-GO poorly fit with the pseudo first-order kinetic model.

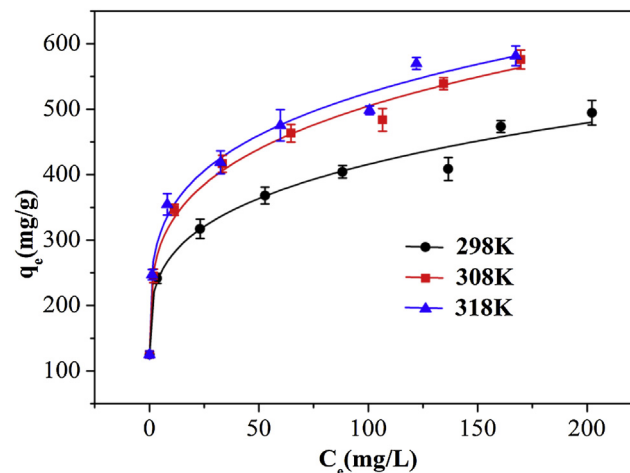


Fig. 8 – Effect of temperature on the adsorption of MB to RL-GO.

Table 1 – Adsorption kinetics parameters of MB onto RL-GO (RL-GO dosage, 400 mg/L; pH value, 7.0; temperature, 298 K).

Concentration (mg/L)	Pseudo-first-order kinetic				Pseudo-second-order kinetic			
	$q_{e,exp}$ (mg/g)	K_1 (1/h)	$q_{e,cal}$ (mg/g)	R^2	$q_{e,exp}$ (mg/g)	k_2 (g/mg.h)	$q_{e,cal}$ (mg/g)	R^2
100	242	0.19	55.31	0.688	242	0.0208	241.55	0.999
150	305	0.28	152.56	0.985	305	0.0068	309.60	0.999
200	365	0.25	127.13	0.926	365	0.0093	364.96	0.999

Pseudo-second-order equation can be expressed by the following equation after integration (Onal et al., 2006):

$$t/q_t = 1/k_2q_e^2 + t/q_e \tag{3}$$

where k_2 (g/mg.h) is the rate constant of pseudo-second-order adsorption determined by plotting t/q_t versus t . The plots of t/q_t against t at different initial MB concentrations are shown in Fig. 9a and the values of parameters are summarized in Table 1. The data shows an excellent fit to pseudo-second-order model with high R^2 (≥ 0.999). A good fit can be further confirmed by the fact that the calculated q_e value is very close to the measured one.

As the above kinetic models were not able to determine the diffusion mechanisms and identify the possible rate controlling procedure that affected the kinetics of adsorption, Intra-particle diffusion and Boyd's film-diffusion model were further examined. Common to the most adsorption processes, intra-particle diffusion model was an empirically functional relationship of adsorption amount at interval t (q_t) with $t^{1/2}$. The rate parameter for intra-particle diffusion was determined by the following equation (Mi et al., 2012):

$$q_t = k_{id}t^{1/2} + C_i \tag{4}$$

Where k_{id} is the intra-particle diffusion rate constant ($\text{mg/g h}^{1/2}$), and C_i is the intercept related to the thickness of the boundary layer, that is, the larger the intercept, the greater the contribution of the surface sorption in the rate controlling. According to this model, if the value of C_i was zero, it means that the rate of adsorption is controlled by intra-particle diffusion for the entire adsorption period. Also, q_t versus $t^{1/2}$ should be linear if intra-particle diffusion was involved in the adsorption process.

For a solid/liquid sorption process, the solute transfer may include the step of either external mass transfer (film diffusion) or intra-particle diffusion, or both. A multi-step process is usually involved in the diffusion mechanism of dye removal from aqueous phase by adsorption (Dawood and Sen, 2012). As shown in Fig. 9b, the plots of q_t against $t^{1/2}$ are multi-linear including three linear sections, which indicates that multiple steps take place during adsorption process. The first section of the curve with a large slope corresponds to transport of MB from the bulk solution to the external surface of RL-GO by film diffusion. The second section describes the gradual adsorption stage, corresponding to the diffusion of the MB molecules from the external surface into the pores of the RL-GO (intra-particle diffusion). The third section with a small slope indicates the final equilibrium stage where the intra-particle diffusion starts to slow down. The model parameters obtained from the sections of plots are listed in Table 2. For all the tested MB concentrations, the values of C_i for each linear portion are not zero, indicating that intra-particle

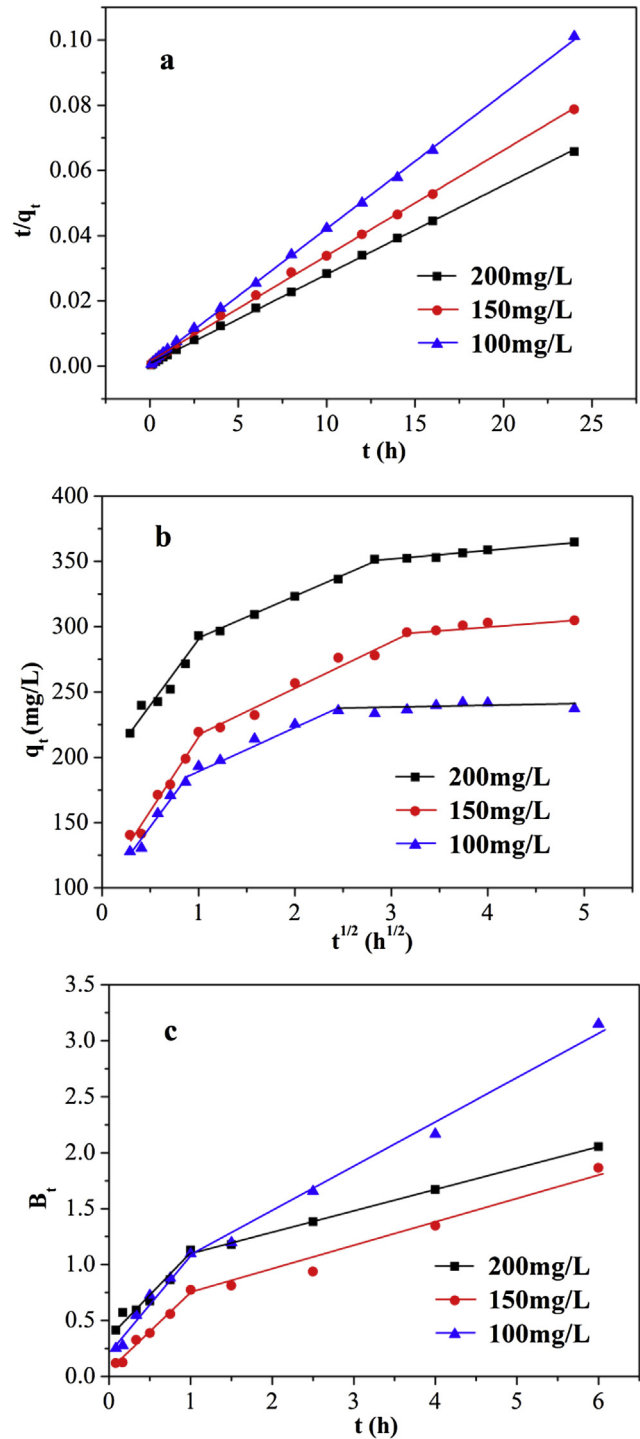


Fig. 9 – (a) Pseudo-second-order plots for MB adsorption, (b) Intra-particle diffusion plots for MB adsorption, (c) Boyd plots for MB adsorption.

Table 2 – Intra-particle diffusion parameters for different initial MB concentrations.

C_0 (mg/L)	K_{1d} (mg/g.h ^{1/2})	K_{2d} (mg/g.h ^{1/2})	K_{3d} (mg/g.h ^{1/2})	C_1	C_2	C_3	$(R_1)^2$	$(R_2)^2$	$(R_3)^2$
100	97.46	30.61	1.91	97.53	162.69	231.41	0.970	0.979	0.871
150	113.96	36.48	5.43	102.04	180.17	279.44	0.969	0.972	0.806
200	94.25	32.31	6.82	192.45	258.71	331.12	0.929	0.994	0.949

diffusion was present as a part of diffusion process, but it is not the sole rate-controlling step in all the stages (Tang et al., 2012). At earlier stages, the adsorption of MB onto RL-GO is controlled due to film diffusion. As the adsorbent particles are loaded with MB ions, the sorption process is controlled due to intra-particle diffusion (Dawood and Sen, 2012).

To gain insights into the actual rate-controlling step involved in the overall MB sorption process, the experimental data was further analyzed using the Boyd model (Boyd et al., 1947):

$$F = 1 - \left(\frac{6}{\pi^2}\right) \exp(-B_t) \quad (5)$$

Where F is the fractional attainment of equilibrium at different time t , and B_t is a mathematical function of F .

$$F = \frac{q_t}{q_e} \quad (6)$$

where q_t and q_e is the MB adsorption quantity (mg/g) at time t and at equilibrium, respectively.

Eq. (5) can be rearranged to:

$$B_t = -0.4977 - \ln(1 - F) \quad (7)$$

Thus the value of B_t can be calculated from Eq. (7) according to each value of F . The linearity of this plot provides a reliable information to identify that the rates of adsorption is controlled by external mass transfer (film diffusion) or intra-particle diffusion. As shown in Fig. 9c, the calculated B_t values are plotted against time t for the first 6 h of MB adsorption onto RL-GO. All the plots show linear relation between B_t and t in the initial phase of adsorption and the regression lines do not pass through the origin, which indicates that film-diffusion controlled the rate of adsorption in the beginning of adsorption, and other mechanisms such as intra-particle diffusion take over and control the rate of adsorption subsequently.

3.7. Adsorption isotherms

For better understanding the thermodynamics of MB adsorption to RL-GO, four adsorption isotherm equations of Langmuir, Freundlich, Temkin and BET were examined based on the adsorption equilibrium data. The linear form of Langmuir equation is (Farghali et al., 2013).

$$\frac{C_e}{q_e} = \frac{C_e}{q_{\max}} + \frac{1}{q_{\max}K_L} \quad (8)$$

Where C_e is the equilibrium concentration of the solution (mg/L), q_e is the amount of dye adsorbed at equilibrium (mg/g), q_{\max} is the maximum adsorption capacity corresponding to complete monolayer coverage (mg/g), K_L is a Langmuir constant

related to the affinity of the binding sites and energy of adsorption (L/mg).

A linear relation is obtained between C_e/q_e and C_e (Fig. 10a), and the Langmuir isotherm constants K_L and q_{\max} are shown in Table 3. Langmuir equation can be used to roughly fit the experimental data with the correlation coefficients $R^2 \geq 0.975$. The q_{\max} and K_L increases with increase in temperature due to the endothermic nature of the adsorption process (Chowdhury et al., 2011). Another parameter R_L , a dimensionless constant separation parameter, is given by the following equation (Weber and Chakravorti, 1974):

$$R_L = \frac{1}{1 + K_L C_0} \quad (9)$$

where C_0 is the highest initial concentration of MB (mg/L). This parameter indicates that the isotherm is unfavorable ($R_L > 1$), favorable ($R_L < 1$), linear ($R_L = 1$), or irreversible ($R_L = 0$) (Hameed, 2008; Wu et al., 2013). In this study, R_L values calculated between 0.016 and 0.055, which proves that the adsorption is a favorable process.

The Freundlich isotherm was an empirical equation which based on that the adsorption process took place on heterogeneous surfaces. The equation is (Liu et al., 2012a):

$$\ln q_e = \ln K_F + \frac{1}{n} \ln C_e \quad (10)$$

where K_F is a Freundlich constant related to adsorption capacity (L/mg), $1/n$ is the heterogeneity factor indicating how favorable the adsorption process is. A linearity between $\ln q_e$ and $\ln C_e$ is obtained, which is shown in Fig. 10b. From the slope and intercept of the regression, the values of Freundlich parameters K_F and n are calculated and listed in Table 3.

The high correlation coefficients ($R^2 \geq 0.991$) for all temperatures tested indicate that the adsorption of methylene blue onto the RL-GO is in compliance with the Freundlich isotherm. The high values of K_F indicate that RL-GO has a high adsorption capacity and affinity for MB. The $1/n$ values are far less than 1, implying that favorable adsorption is for MB onto RL-GO at all temperatures studied. The increase of Freundlich constants (K_F) with increase of temperature suggests that high temperature favors adsorption and the adsorption is endothermic in nature.

The Temkin isotherm was based on an assumption that there is indirect adsorbate–adsorbate interaction for adsorption. The heat of adsorption decreases linearly with coverage due to this interaction. The linearized form of this isotherm is (Njoku et al., 2014):

$$q_e = B_T \ln K_T + B_T \ln C_e \quad (11)$$

where $B_T = RT/b_T$ and b_T (J/mol) is the Temkin constant related to the heat of adsorption, R is the universal gas constant (8.314 J/mol.K) and T is the temperature (K); K_T (L/mg) is the maximum binding energy constant; q_e (mg/g) and C_e (mg/L) is

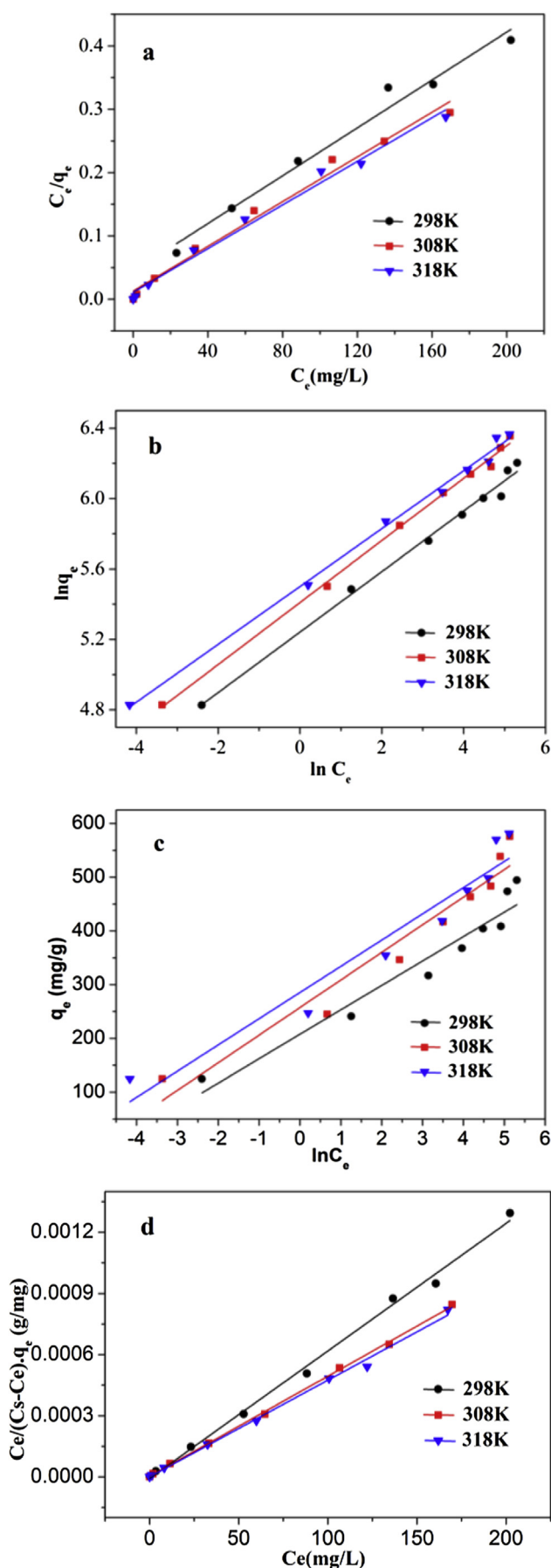


Table 3 – Isotherm parameters for the adsorption of MB onto RL-GO.

Isotherms	Parameters	Temperature (K)		
		298	308	318
Langmuir	q_{max} (mg/g)	529.10	568.18	581.40
	K_L (L/mg)	0.04	0.14	0.16
	R^2	0.975	0.986	0.987
Freundlich	R_L	0.055	0.018	0.016
	$1/n$	0.17	0.18	0.16
	K_F (L/mg)	188.96	233.53	244.84
Tempkin	R^2	0.991	0.996	0.995
	K_T (L/mg)	96.62	150.30	348.03
	B_T	45.44	51.35	48.77
	R^2	0.928	0.931	0.925
BET	B_T (J/mol)	54.52	49.86	54.21
	K_b	-414.81	1148.75	171,84.23
	q_m (mg/g)	309.17	392.11	406.82
	R^2	0.995	0.999	0.996

the amount of adsorbate adsorbed onto adsorbent and the adsorbate concentration at equilibrium, respectively. A linear regression plot of q_e versus $\ln C_e$ is shown in Fig. 10c, and the calculated values of B_T , b_T and K_T are included in Table 3. It is found that the plots of Tempkin are deviate from linearity at all the temperatures. The correlation coefficients (R^2) estimated by related plots are ranged from 0.925 to 0.931. The lower value of b_T indicates that the interaction between MB and RL-GO is weak.

As an improvement on the Langmuir model, the BET adsorption model was based on the assumption that adsorbate could be adsorbed onto the adsorbent surface forming multi-layer in a random distribution of adsorbed particle (Hussain et al., 2013). It also presumed that adsorption energy and condensation energy were responsible for the first monolayer and for the adsorption of successive layers, respectively. The linear form of the BET equation is (Arami et al., 2006):

$$\frac{C_e}{(C_s - C_e)q_e} = \frac{1}{K_b q_m} + \frac{C_e(K_b - 1)}{K_b q_m C_s} \tag{12}$$

Where C_e is the equilibrium concentration of adsorbate in solution (mg/L), C_s is saturation concentration of solute (mg/L), q_e is the final amount of adsorbate adsorbed onto adsorbent (mg/g), q_m is the amount of solute adsorbed in forming a complete monolayer (mg/g), K_b is the BET constant. The plots of $C_e/(C_s - C_e) \cdot q_e$ versus C_e at different temperature are shown in Fig. 10d, and all relevant parameters are listed in Table 3. The high correlation coefficients ($R^2 > 0.995$) indicate that the BET model fits MB adsorption on RL-GO ideally. The results also provide an information that the adsorption of MB onto the surface of RL-GO may be in multilayer formation (Jahangiri-Rad et al., 2013).

3.8. Thermodynamic study

To further estimate the effect of temperature on the adsorption of MB onto RL-GO, the thermodynamic parameters

Fig. 10 – The equilibrium isotherms for MB adsorbed by RL-GO: (a) the Langmuir model; (b) the Freundlich model; (c) The Temkin model; (d) The BET model.

involving Gibbs free energy (ΔG^0), enthalpy (ΔH^0), and entropy (ΔS^0) were determined by following equations (Wang et al., 2013b):

$$\Delta G^0 = -RT \ln b \quad (13)$$

$$\Delta H^0 = RT_2 T_1 / T_2 - T_1 \ln(b_2 / b_1) \quad (14)$$

$$\Delta S^0 = \Delta H^0 - \Delta G^0 / T \quad (15)$$

Where R (8.314 J/mol K) is the universal gas constant. T (K) is the absolute temperature, and b is Langmuir constant (the unit of k_L should be transformed into milligrams per gram for the calculation of ΔG^0) at a temperature T. From Table 4, the negative values of ΔG^0 are found to decrease from -26.345 to -31.504 kJ/mol with the temperature increase in the range of 298–318 K. This once again indicates that the MB adsorption process is spontaneous and becomes more favorable at higher temperatures (Luo et al., 2010). In general, the value of energy ΔG^0 in between 0 and -20 kJ/mol suggests that the adsorption process is physisorption, while the value in between -80 and -400 kJ/mol corresponds to chemisorptions (Wu et al., 2013). Thus, based on the values of ΔG^0 , the adsorption of MB onto RL-GO may involve both physisorption and chemisorption. The positive ΔH^0 value implies that the adsorption is endothermic, which is also supported by the study for effect of temperature. The positive value of ΔS^0 indicates that randomness at the solid/solution interface increased during the adsorption process, which reflects some structural changes of dyes and RL-GO (Zhao et al., 2011b).

3.9. Adsorption mechanisms

As discussed in the effect of pH on MB adsorption, the electrostatic attraction is regarded as the main adsorption force. However, the adsorption process often includes a complex adsorption mechanism and various types of interactions may be involved in MB adsorption onto the RL-GO. To verify the adsorption mechanism, the FT-IR spectrums (Fig. 11a) of RL-GO, MB and MB loaded RL-GO (RL-GO/MB) were investigated. After the adsorption of MB onto RL-GO, the FT-IR spectrum exhibits many changes. The adsorption band of RL-GO at 1691 and 1740 cm^{-1} corresponding to C=O for $-\text{COOH}$ slightly shift to 1687 and 1734 cm^{-1} , respectively, indicating that carboxyl of RL-GO plays an important role in the adsorption process ascribed to its ionization which makes the surface of RL-GO negatively charged. It also can be seen that the adsorption peaks (at 1645 and 3427 cm^{-1}) belonged to C=C and O-H for RL-GO migrate to wavenumbers 1652 and 3420 cm^{-1} , respectively, which suggests that other adsorption mechanisms

such as π - π interaction and hydrogen bond, could be involved in MB adsorption (Fu et al., 2015; Wu et al., 2014). Furthermore, the characteristic adsorption peaks of MB at 826, 880 and 1589 cm^{-1} ascribed to the aromatic rings shift to 831, 883 and 1598 cm^{-1} , respectively. This result confirms the presence of π - π interaction as each carbon atom in GO of RL-GO sheet has a π electron orbit which is perpendicular to the surface, and MB molecules containing C=C double bonds and benzene rings with π electrons could form π - π bond with RL-GO (Wang et al., 2013c). Besides, for MB, the C-N stretching vibration at 1319 and 1389 cm^{-1} shifts to 1334 and 1392 cm^{-1} , respectively. The information testifies the existence of hydrogen bond between hydroxyl of RL-GO and nitrogen of MB (Liu et al., 2012b). The molecule interactions between RL-GO and MB discussed above during the adsorption process are schematically represented in Fig. 11b.

3.10. Comparison with other adsorbents

The comparisons of maximum adsorption capacities of the RL-GO composite obtained in this work with various adsorbents previously studied for the adsorption of MB are listed in Table 5. As can be seen, the MB adsorption capacity of RL-GO composite is 529.10 mg/g at 298 K, which is higher than that of GO studied in this paper. Furthermore, this value is also much higher than other adsorbents such as cotton stalk (Deng et al., 2011), carbon nanotube (Yao et al., 2010), graphene (Liu et al., 2012a), graphene coated biochar (Zhang et al., 2012), graphene oxide (Li et al., 2013a) and magnetic chitosan/graphene oxide (Fan et al., 2012). Such comparison suggests that RL-GO may be an effective adsorbent for MB removal from contaminated water.

3.11. Application of RL-GO to real water samples

To test the effect of RL-GO in MB removal from real water subjected to MB contamination, tap water, river water and dye wastewater were used as the matrices of the adsorption solution, and the results are shown in Table 6. It is observed that the adsorption capacity for MB in tap water, river water and dye wastewater are higher than that in lab ultrapure water when initial MB concentration is 100 or 200 mg/L. Particularly, in river water and dye wastewater with 200 mg/L MB, the adsorption capacity of RL-GO is 476.05 and 497.8 mg/g, respectively, and the corresponding removal percentage reaches up to 95.21% and 99.56%. This high MB removal efficiency of RL-GO in dye wastewater may result from a higher pH, and it indicates the great application potential of RL-GO in removing MB from dye wastewater.

3.12. The cost analysis and renewability evaluation

As rhamnolipid is a microbial metabolite, the wholesale price of rhamnolipid with high purity is approximately US\$ 24 $\times 10^4$ per ton. The graphene oxide used in the experiment was prepared from graphite powder (US\$ 1.7 $\times 10^3$ per ton) and other raw materials can be cheaply obtained from industrial supplies. Thus, the cost of RL-GO prepared in this work is dramatically affected by the biosurfactant rhamnolipid consumed. The corresponding price of consumed

Table 4 – Thermodynamic parameters for MB adsorption on RL-GO.

T (K)	ΔG^0 (kJ/mol)	ΔS^0 (J/(K mol))	ΔH^0 (kJ/mol)
298	-26.35	255.17	49.44
308	-30.16	259.30	
318	-31.50	258.61	

The value of ΔH^0 listed is an average value.

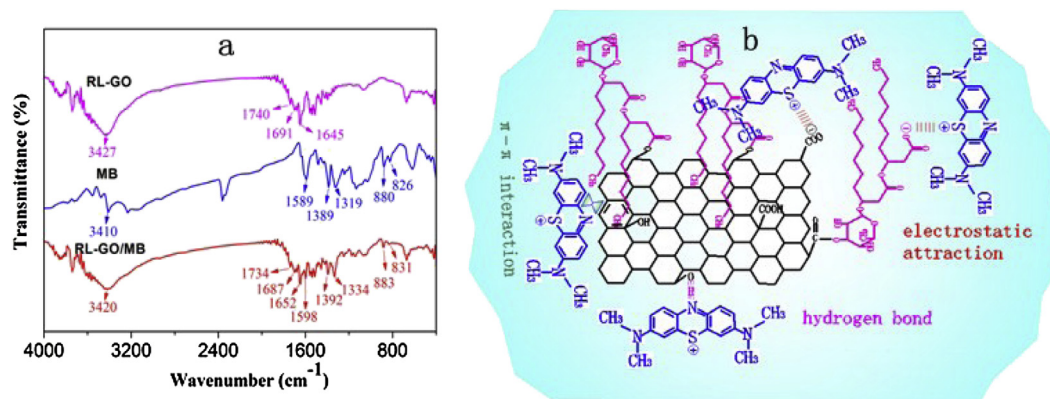


Fig. 11 – (a) FT-IR spectra of RL-GO, MB and RL-GO/MB; (b) Schematic illustration of adsorption mechanisms by RL-GO.

rhamnolipid would be approximately US\$ 60×10^4 for producing one metric ton of RL-GO. Comparison with single-walled carbon nanotubes (US\$ 441.85×10^6 /t) (Shawky et al., 2012), multi-walled carbon nanotubes (US\$ 2.5×10^6 /t) (Wang et al., 2014), carboxyl multi-walled carbon nanotubes (US\$ 70×10^6 /t) (Shawky et al., 2012) and C18 silica (US\$ 400×10^4 /t) (El-Sheikh et al., 2008), the cost of our prepared adsorbents is much lower. Furthermore, the recyclability is an important factor for evaluating the economy and applicability

of adsorbents (Dawood and Sen, 2012). The regeneration and reusability of RL-GO is investigated and the RL-GO should be able to be reused through a large number of water treatment and regeneration cycles, and then, it can possibly be cost-effective adsorbents. From Fig. 12, it can be informed that the adsorbed amount of MB onto the as prepared RL-GO is 321.56 mg/L at the natural pH (5.87). After five adsorption/desorption cycles, the adsorbed amount of MB onto the recycled RL-GO sheets still remains at 313.47 mg/L, which only reduces by 2.52% compared to that of the first cycle. The results indicate that the RL-GO could be a cost-effective, efficient and potential adsorbent for MB removal due to the excellent regeneration performance.

Table 5 – Maximum adsorption capacities for MB onto various adsorbents.

Adsorbent	pH	Temp (K)	q_{max} (mg/g)	References
Cotton stalk	7.0	308	147.06	(Deng et al., 2011)
Powdered activated carbon	7.0	293	91.00	(Yener et al., 2008)
Carbon nanotube	7.0	298	46.20	(Yao et al., 2010)
Graphene	3.0	293	153.85	(Liu et al., 2012)
Graphene oxide	6.0	298	243.90	(Li et al., 2013a)
Graphene coated biochar		295	174	(Zhang et al., 2012)
Magnetic chitosan/graphene oxide	5.3	303	95.16	(Fan et al., 2012)
Graphene/carbon nanotube			81.97	(Ai and Jiang, 2012)
Graphene oxide/calcium alginate	5.4	298	181.81	(Li et al., 2013b)
GO	7.0	298	377.63	In this study
RL-GO	7.0	298	529.10	In this study

Table 6 – Efficiency of MB removal by RL-GO from real watersamples (RL-GO, 400 mg/L; contact time, 24 h; temperature, 298 K).

Initial MB concentration in solution (mg/L)	100		200	
	q_e (mg/g)	Removal (%)	q_e (mg/g)	Removal (%)
Ultrapure water (pH 6.0)	234.40	93.76	331.21	66.24
Tap water (pH 7.2)	248.48	99.39	468.55	93.71
River water (pH 7.4)	248.82	99.53	476.05	95.21
Dye wastewater (pH 8.3)	249.36	99.75	497.80	99.56

4. Conclusions

A novel adsorbent of RL-GO with super adsorption capacity is synthesized by one-step ultrasonication for the removal of MB from aqueous solution. The as-prepared RL-GO has a mesopores structure, negative charged surface in pH range between 4.0–11.0 and rich oxygen-containing functional groups. The adsorption process of MB fits the pseudo-second-order kinetic model very well, and the diffusion mechanism involves a

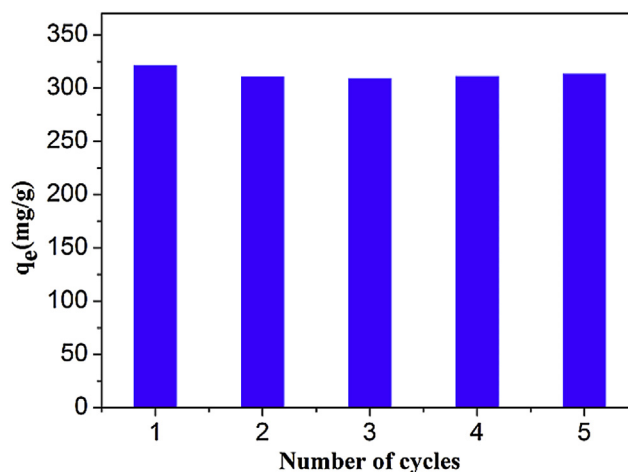


Fig. 12 – Reusability of the RL-GO for MB removal.

multi-step process. The BET isotherm model as well as Freundlich isotherm model yields a much better fit than that of Langmuir isotherm model and Temkin isotherm in describing MB adsorption. The MB maximum adsorption capacity of RL-GO calculated from the Langmuir model is 529.10, 568.18 and 581.40 mg/g at 298 K, 308 and 318 K, respectively, and it is strongly dependent on adsorbent dosage, pH, temperature and initial concentration. The adsorption of MB is a spontaneous and endothermic of physisorption and chemisorptions process ascribing to the electrostatic attraction, π - π interaction and hydrogen band between RL-GO and MB. The RL-GO could be a cost-effective, efficient and potential adsorbent due to its excellent reusability and outstanding performance in MB removal from real wastewater.

Acknowledgments

This work was supported by the National Natural Science Foundation of China (501100001809) (No. 21276069, 51378192, 71431006), the Fundamental Research Funds for the Central Universities, the Hunan Province Innovation Foundation for Postgraduate (No. CX2014B142), and the Collaborative Innovation Center of Resource conserving & Environment-friendly Society and Ecological Civilization-China.

REFERENCES

- Ai, L., Jiang, J., 2012. Removal of methylene blue from aqueous solution with self-assembled cylindrical graphene-carbon nanotube hybrid. *Chem. Eng. J.* 192, 156–163.
- Anbia, M., Salehi, S., 2012. Removal of acid dyes from aqueous media by adsorption onto amino-functionalized nanoporous silica SBA-3. *Dyes Pigments* 94 (1), 1–9.
- Arami, M., Yousefi Limaee, N., Mahmoodi, N.M., 2006. Investigation on the adsorption capability of egg shell membrane towards model textile dyes. *Chemosphere* 65 (11), 1999–2008.
- Asci, Y., Nurbas, M., Acikel, Y.S., 2008. Removal of zinc ions from a soil component Na-feldspar by a rhamnolipid biosurfactant. *Desalination* 223 (1–3), 361–365.
- Bianco, A., 2013. Graphene: safe or toxic? The two faces of the medal. *Angew. Chem. Int. Ed. Engl.* 52 (19), 4986–4997.
- Boyd, G.E., Adamson, A.W., Myers, I.S., 1947. The exchange adsorption of ions from aqueous solutions by organic zeolites; kinetics. *J. Am. Chem. Soc.* 69, 2836–2848.
- Chang, Y., Ren, C., Qu, J., Chen, X., 2012. Preparation and characterization of Fe₃O₄/graphene nanocomposite and investigation of its adsorption performance for aniline and p-chloroaniline. *Appl. Surf. Sci.* 261, 504–509.
- Chen, L., Hu, P., Zhang, L., Huang, S., Luo, L., Huang, C., 2012. Toxicity of graphene oxide and multi-walled carbon nanotubes against human cells and zebrafish. *Sci. China Chem.* 55 (10), 2209–2216.
- Chowdhury, S., Mishra, R., Saha, P., Kushwaha, P., 2011. Adsorption thermodynamics, kinetics and isosteric heat of adsorption of malachite green onto chemically modified rice husk. *Desalination* 265 (1–3), 159–168.
- Dawood, S., Sen, T.K., 2012. Removal of anionic dye Congo red from aqueous solution by raw pine and acid-treated pine cone powder as adsorbent: equilibrium, thermodynamic, kinetics, mechanism and process design. *Water Res.* 46 (6), 1933–1946.
- Deng, H., Lu, J., Li, G., Zhang, G., Wang, X., 2011. Adsorption of methylene blue on adsorbent materials produced from cotton stalk. *Chem. Eng. J.* 172 (1), 326–334.
- Dong, Y., Han, Z., Liu, C., Du, F., 2010. Preparation and photocatalytic performance of Fe (III)-amidoximated PAN fiber complex for oxidative degradation of azo dye under visible light irradiation. *Sci. Total Environ.* 408 (10), 2245–2253.
- El-Sheikh, A.H., Sweileh, J.A., Al-Degs, Y.S., Insisi, A.A., Al-Rabady, N., 2008. Critical evaluation and comparison of enrichment efficiency of multi-walled carbon nanotubes, C18 silica and activated carbon towards some pesticides from environmental waters. *Talanta* 74 (5), 1675–1680.
- Fan, L., Luo, C., Li, X., Lu, F., Qiu, H., Sun, M., 2012. Fabrication of novel magnetic chitosan grafted with graphene oxide to enhance adsorption properties for methyl blue. *J. Hazard Mater.* 215–216, 272–279.
- Farghali, A.A., Bahgat, M., El Rouby, W.M.A., Khedr, M.H., 2013. Preparation, decoration and characterization of graphene sheets for methyl green adsorption. *J. Alloys Compd.* 555, 193–200.
- Fu, J., Chen, Z., Wang, M., Liu, S., Zhang, J., Zhang, J., Han, R., Xu, Q., 2015. Adsorption of methylene blue by a high-efficiency adsorbent (polydopamine microspheres): kinetics, isotherm, thermodynamics and mechanism analysis. *Chem. Eng. J.* 259, 53–61.
- Ghosh, T., Ullah, K., Nikam, V., Park, C.Y., Meng, Z.D., Oh, W.C., 2013. The characteristic study and sonocatalytic performance of CdSe-graphene as catalyst in the degradation of azo dyes in aqueous solution under dark conditions. *Ultrason. Sonochem.* 20 (2), 768–776.
- Gusmao, K.A., Gurgel, L.V., Melo, T.M., Gil, L.F., 2013. Adsorption studies of methylene blue and gentian violet on sugarcane bagasse modified with EDTA dianhydride (EDTAD) in aqueous solutions: kinetic and equilibrium aspects. *J. Environ. Manage* 118, 135–143.
- Hameed, B.H., 2008. Equilibrium and kinetic studies of methyl violet sorption by agricultural waste. *J. Hazard Mater.* 154 (1–3), 204–212.
- Hummers, W.S., Offeman, R.E., 1958. Preparation of graphitic oxide. *J. Am. Chem. Soc.* 80, 1339.
- Hussain, S., van Leeuwen, J., Chow, C., Beecham, S., Kamruzzaman, M., Wang, D., Drikas, M., Aryal, R., 2013. Removal of organic contaminants from river and reservoir waters by three different aluminum-based metal salts: Coagulation adsorption and kinetics studies. *Chem. Eng. J.* 225, 394–405.
- Jahangiri-Rad, M., Nadafi, K., Mesdaghinia, A., Nabizadeh, R., Younesian, M., Rafiee, M., 2013. Sequential study on reactive blue 29 dye removal from aqueous solution by peroxy acid and single wall carbon nanotubes: experiment and theory. *Iran. J. Environ. Health Sci. Eng.* 10 (1), 5.
- Khatti, S.D., Singh, M.K., 2009. Removal of malachite green from dye wastewater using neem sawdust by adsorption. *J. Hazard Mater.* 167 (1–3), 1089–1094.
- Lagergren, S., 1898. Zur theorie der sogenannten adsorption gelöster Stoffe. *Stockholm Kongl. svenska vetenskaps-akad. Handlingar* 24 (4), 1–39.
- Li, Y., Du, Q., Liu, T., Peng, X., Wang, J., Sun, J., Wang, Y., Wu, S., Wang, Z., Xia, Y., Xia, L., 2013a. Comparative study of methylene blue dye adsorption onto activated carbon, graphene oxide, and carbon nanotubes. *Chem. Eng. Res. Des.* 91 (2), 361–368.
- Li, Y., Du, Q., Liu, T., Sun, J., Wang, Y., Wu, S., Wang, Z., Xia, Y., Xia, L., 2013b. Methylene blue adsorption on graphene oxide/calcium alginate composites. *Carbohydr. Polym.* 95 (1), 501–507.
- Lin, S., Shih, C.J., Strano, M.S., Blankschtein, D., 2011. Molecular insights into the surface morphology, layering structure, and

- aggregation kinetics of surfactant-stabilized graphene dispersions. *J. Am. Chem. Soc.* 133 (32), 12810–12823.
- Liu, R., Zhang, B., Mei, D., Zhang, H., Liu, J., 2011. Adsorption of methyl violet from aqueous solution by halloysite nanotubes. *Desalination* 268 (1–3), 111–116.
- Liu, T., Li, Y., Du, Q., Sun, J., Jiao, Y., Yang, G., Wang, Z., Xia, Y., Zhang, W., Wang, K., Zhu, H., Wu, D., 2012a. Adsorption of methylene blue from aqueous solution by graphene. *Colloids Surf. B Biointerfaces* 90, 197–203.
- Liu, X., Zhang, H., Ma, Y., Wu, X., Meng, L., Guo, Y., Yu, G., Liu, Y., 2013. Graphene-coated silica as a highly efficient sorbent for residual organophosphorus pesticides in water. *J. Mater. Chem. A* 1 (5), 1875.
- Liu, Y., Wang, J., Zheng, Y., Wang, A., 2012b. Adsorption of methylene blue by kapok fiber treated by sodium chlorite optimized with response surface methodology. *Chem. Eng. J.* 184, 248–255.
- Luo, P., Zhao, Y., Zhang, B., Liu, J., Yang, Y., Liu, J., 2010. Study on the adsorption of neutral red from aqueous solution onto halloysite nanotubes. *Water Res.* 44 (5), 1489–1497.
- Mi, X., Huang, G., Xie, W., Wang, W., Liu, Y., Gao, J., 2012. Preparation of graphene oxide aerogel and its adsorption for Cu²⁺ ions. *Carbon* 50 (13), 4856–4864.
- Nethaji, S., Sivasamy, A., Thennarasu, G., Saravanan, S., 2010. Adsorption of Malachite Green dye onto activated carbon derived from *Borassus aethiopum* flower biomass. *J. Hazard Mater.* 181 (1–3), 271–280.
- Njoku, V.O., Foo, K.Y., Asif, M., Hameed, B.H., 2014. Preparation of activated carbons from rambutan (*Nephelium lappaceum*) peel by microwave-induced KOH activation for acid yellow 17 dye adsorption. *Chem. Eng. J.* 250, 198–204.
- Onal, Y., Akmil-Basar, C., Eren, D., Sarici-Ozdemir, C., Depci, T., 2006. Adsorption kinetics of malachite green onto activated carbon prepared from Tuncbilek lignite. *J. Hazard Mater.* 128 (2–3), 150–157.
- Ong, S.A., Toorisaka, E., Hirata, M., Hano, T., 2005. Biodegradation of redox dye Methylene Blue by up-flow anaerobic sludge blanket reactor. *J. Hazard Mater.* 124 (1–3), 88–94.
- Paredes, J.I., Villar-Rodil, S., Martinez-Alonso, A., Tascon, J.M.D., 2008. Graphene oxide dispersions in organic solvents. *Langmuir* 24, 10560–10564.
- Qu, G., Wang, X., Liu, Q., Liu, R., Yin, N., Ma, J., Chen, L., He, J., Liu, S., Jiang, G., 2013. The ex vivo and in vivo biological performances of graphene oxide and the impact of surfactant on graphene oxide's biocompatibility. *J. Environ. Sci.* 25 (5), 873–881.
- Rahchamani, J., Mousavi, H.Z., Behzad, M., 2011. Adsorption of methyl violet from aqueous solution by polyacrylamide as an adsorbent: isotherm and kinetic studies. *Desalination* 267 (2–3), 256–260.
- Ramesha, G.K., Kumara, A.V., Muralidhara, H.B., Sampath, S., 2011. Graphene and graphene oxide as effective adsorbents toward anionic and cationic dyes. *J. Colloid Interface Sci.* 361 (1), 270–277.
- Shawky, H.A., El-Aassar, A.H.M., Abo-Zeid, D.E., 2012. Chitosan/carbon nanotube composite beads: preparation, characterization, and cost evaluation for mercury removal from wastewater of some industrial cities in Egypt. *J. Appl. Polym. Sci.* 125 (S1), E93–E101.
- Tang, H., Zhou, W., Zhang, L., 2012. Adsorption isotherms and kinetics studies of malachite green on chitin hydrogels. *J. Hazard Mater.* 209–210, 218–225.
- Tang, Q., Zhou, Z., Chen, Z., 2013. Graphene-related nanomaterials: tuning properties by functionalization. *Nanoscale* 5 (11), 4541–4583.
- Tiwari, J.N., Mahesh, K., Le, N.H., Kemp, K.C., Timilsina, R., Tiwari, R.N., Kim, K.S., 2013. Reduced graphene oxide-based hydrogels for the efficient capture of dye pollutants from aqueous solutions. *Carbon* 56, 173–182.
- Wang, H., Yuan, X., Wu, Y., Huang, H., Peng, X., Zeng, G., Zhong, H., Liang, J., Ren, M., 2013a. Graphene-based materials: fabrication, characterization and application for the decontamination of wastewater and wastegas and hydrogen storage/generation. *Adv. Colloid Interface Sci.* 195–196, 19–40.
- Wang, H., Yuan, X., Wu, Y., Huang, H., Zeng, G., Liu, Y., Wang, X., Lin, N., Qi, Y., 2013b. Adsorption characteristics and behaviors of graphene oxide for Zn(II) removal from aqueous solution. *Appl. Surf. Sci.* 279, 432–440.
- Wang, K., Ruan, J., Song, H., Zhang, J., Wo, Y., Guo, S., Cui, D., 2011. Biocompatibility of graphene oxide. *Nanoscale Res. Lett.* 6 (1), 1–8.
- Wang, P., Cao, M., Wang, C., Ao, Y., Hou, J., Qian, J., 2014. Kinetics and thermodynamics of adsorption of methylene blue by a magnetic graphene-carbon nanotube composite. *Appl. Surf. Sci.* 290, 116–124.
- Wang, Y., Wang, W., Wang, A., 2013c. Efficient adsorption of methylene blue on an alginate-based nanocomposite hydrogel enhanced by organo-illite/smectite clay. *Chem. Eng. J.* 228, 132–139.
- Wang, Y., Zeng, L., Ren, X., Song, H., Wang, A., 2010. Removal of Methyl Violet from aqueous solutions using poly (acrylic acid-co-acrylamide)/attapulgitite composite. *J. Environ. Sci.* 22 (1), 7–14.
- Weber, T.W., Chakravorti, R.K., 1974. Pore and solid diffusion models for fixed-bed adsorbents. *AIChE J.* 20, 228–237.
- Wu, J.N., Eiteman, M.A., Law, S.E., 1998. Evaluation of membrane filtration and ozonation processes for treatment of reaction dye wastewater. *J. Environ. Eng.* 124, 272–277.
- Wu, Y., Luo, H., Wang, H., Wang, C., Zhang, J., Zhang, Z., 2013. Adsorption of hexavalent chromium from aqueous solutions by graphene modified with cetyltrimethylammonium bromide. *J. Colloid Interface Sci.* 394, 183–191.
- Wu, Z., Zhang, L., Guan, Q., Ning, P., Ye, D., 2014. Preparation of α -zirconium phosphate-pillared reduced graphene oxide with increased adsorption towards methylene blue. *Chem. Eng. J.* 258, 77–84.
- Xu, J., Wang, L., Zhu, Y., 2012. Decontamination of bisphenol A from aqueous solution by graphene adsorption. *Langmuir* 28 (22), 8418–8425.
- Yan, J., Chen, G., Cao, J., Yang, W., Xie, B., Yang, M., 2012. Functionalized graphene oxide with ethylenediamine and 1,6-hexanediamine. *New. Carbon Mater.* 27 (5), 370–376.
- Yang, S.T., Chen, S., Chang, Y., Cao, A., Liu, Y., Wang, H., 2011. Removal of methylene blue from aqueous solution by graphene oxide. *J. Colloid Interface Sci.* 359 (1), 24–29.
- Yao, Y., Xu, F., Chen, M., Xu, Z., Zhu, Z., 2010. Adsorption behavior of methylene blue on carbon nanotubes. *Bioresour. Technol.* 101 (9), 3040–3046.
- Yener, J., Kopac, T., Dogu, G., Dogu, T., 2008. Dynamic analysis of sorption of Methylene Blue dye on granular and powdered activated carbon. *Chem. Eng. J.* 144 (3), 400–406.
- Zhang, M., Gao, B., Yao, Y., Xue, Y., Inyang, M., 2012. Synthesis, characterization, and environmental implications of graphene-coated biochar. *Sci. Total Environ.* 435–436, 567–572.
- Zhang, W., Zhou, C., Zhou, W., Lei, A., Zhang, Q., Wan, Q., Zou, B., 2011. Fast and considerable adsorption of methylene blue dye onto graphene oxide. *Bull. Environ. Contam. Toxicol.* 87 (1), 86–90.
- Zhao, G., Li, J., Ren, X., Chen, C., Wang, X., 2011a. Few-layered graphene oxide nanosheets as superior sorbents for heavy metal ion pollution management. *Environ. Sci. Technol.* 45 (24), 10454–10462.
- Zhao, G., Li, J., Wang, X., 2011b. Kinetic and thermodynamic study of 1-naphthol adsorption from aqueous solution to sulfonated graphene nanosheets. *Chem. Eng. J.* 173 (1), 185–190.
- Zhao, G., Wen, T., Yang, X., Yang, S., Liao, J., Hu, J., Shao, D., Wang, X., 2012. Preconcentration of U(VI) ions on few-layered

- graphene oxide nanosheets from aqueous solutions. *Dalton Trans.* 41 (20), 6182–6188.
- Zhao, J., Wang, Z., Zhao, Q., Xing, B., 2014. Adsorption of phenanthrene on multilayer graphene as affected by surfactant and exfoliation. *Environ. Sci. Technol.* 48 (1), 331–339.
- Zhu, M., Li, Z., Xiao, B., Lu, Y., Du, Y., Yang, P., Wang, X., 2013. Surfactant assistance in improvement of photocatalytic hydrogen production with the porphyrin noncovalently functionalized graphene nanocomposite. *ACS Appl. Mater. Interfaces* 5 (5), 1732–1740.